Enhanced antibacterial activity of carbon dots functionalized with ampicillin combined with visible light triggered photodynamic effects

Roxana Jijie, Alexandre Barras, Julie Bouckaert, Nicoleta Dumitrascu, Sabine Szunerits, Rabah Boukherroub

Enhanced antibacterial activity of carbon dots functionalized with ampicillin combined with visible light triggered photodynamic effects

Roxana Jijie,[1,2] Alexandre Barras,[1] Julie Bouckaert,[3] Nicoleta Dumitrascu,[2] Sabine Szunerits[1] and Rabah Boukherroub[1*]

[1]*Univ. Lille, CNRS, Central Lille, ISEN, Univ. Valenciennes, UMR 8520, IEMN, F-59000 Lille, France*

[2]*Iasi Plasma Advanced Research Center (IPARC), Faculty of Physics, AlexandruIoanCuza University of Iasi, Bd. Carol I no. 11, Iasi, 700506, Romania*

[3]*Unité de Glycobiologie Structurale et Fonctionnelle (UGSF), UMR 8576 du CNRS et Université Lille, 50 Av. de Halley, 59658 Villeneuve d'Ascq, France*

Abstract

In the last years, carbon-based nanomaterials have attracted considerable attention in a wide range of fields, particularly in biomedicine, owing to their remarkable photo-physical and chemical properties. In this study, we demonstrate that amine-terminated carbon dots (CDs-NH_2) functionalized with ampicillin (AMP) offer a new perspective for antibacterial treatment. The amine-functionalized carbon dots were used as a carrier for immobilization and delivery of ampicillin (CDs-AMP) and as a visible light-triggered antibacterial material. Additionally, AMP immobilization on the CDs-NH_2 surface improves its stability in solution as compared to free AMP. The AMP conjugated CDs platform combines the antibacterial function of AMP and conserves the intrinsic theranostic properties of CDs-NH_2. Therefore, the AMP immobilized onto CDs-NH_2 surface together with the generation of moderate quantities of reactive oxygen species under visible light illumination is very effective to inactivate the growth of *Escherichia coli*.

Keywords*: Carbon dots; Ampicillin; Bactericidal activity; Escherichia coli; PDT*

[*]To whom correspondence should be sent: rabah.boukherroub@univ-lille1.fr

1. Introduction

The increase of multidrug-resistant bacteria infections represents an important biomedical challenge, demanding the development of alternative antibacterial-based platforms for which pathogens will not be able to develop resistance. In some situations, even the aggressive antibiotic treatment is not able to eradicate the infection due to the ability of bacteria to form biofilms.

In recent years, antimicrobial nanoparticles (NPs) [1], nano-sized carriers for the delivery of therapeutic agents [2] or light-responsive NPs [3-5] offer new approaches to fight against infectious diseases. Among the various nanoparticles, fluorescent carbon dots (CDs) open promising avenues for bacteria detection, imaging and inactivation due their remarkable optical properties, their surface versatility and good biocompatibility [6-14]. For example, Mehta *et al.*[11] reported that CDs, synthesized by using *S. officinarum* juice at 120 °C, acted as excellent fluorescent probes for imaging of *Escherichia coli* (*E. coli*) bacteria. Amphiphilic CDs [7] and PEG-passivated CDs [12] revealed also their potential as fluorescent markers for bacterial detection and imaging. Zhong *et al.* [13] employed CDs modified with vancomycin for assaying *Staphylococcus aureus (S. aureus)*. Dou *et al.* [14] showed that quaternary linear and branched polyethyleneimine passivated CDs exhibit promising antibacterial activity against both Gram-negative and Gram-positive bacteria.

Up to date, a limited attention has been paid for the use of fluorescent CDs as drug delivery vehicles [8, 15-18]. This also applies for their application for photodynamic/photothermal (PDT/PTT) therapy and particularly when it comes to the treatment of bacterial infections. The advantage of antimicrobial PDT includes equal killing efficiency independent of antibiotic resistance, the repetition of therapy without cumulative toxicity, and high spatial control. There has been much effort in the design of effective platforms for the treatment of cancer using CDs in combination with conventional photosynthesizers (PS) such as protoporphyrin I [19] or zinc phthalocyanine [20], while less effort has been devoted to the intrinsic photodynamic and/or antibacterial properties of CDs. The effect of surface charge (negative, neutral and positive) of CDs on the growth of *Escherichia coli (E. coli)* and the mechanism of antibacterial activity induced by these carbon nanostructures was investigated by Bing and coworkers [21]. Upon 6 h incubation of *E. coli* with the CDs, it was found that the positively charged CDs exhibited the strongest bactericidal activity, while the negatively charged and uncharged CDs had almost no

bactericidal activity. A mechanistic study revealed that the bacteria exhibited characteristic markers of apoptosis upon treatment with the positively and negatively charged CDs, similar to those encountered upon treatment with common antibiotics [21]. CDs, prepared from Metronidazole (a wide spectrum antibiotic against obligate anaerobes, including *Peptostreptococcus micros*, *Prevotella intermedia, P. gingvivalis* and *Fusobacterium*) as the carbon source using hydrothermal conditions, displayed inhibition growth of *P. gingvivalis* [22]. Yang *et al.* [23] prepared quaternary ammonium functionalized CDs by conjugating lauryl betaine (BS-12) to amine-terminated CDs using the common NHS/EDC coupling chemistry. The developed material exhibited good fluorescence emission for simultaneous detection and inhibition of Gram-positive bacteria. Sattarahmady *et al.* [24] demonstrated that the bactericidal effect of CDs can be accelerated by near infrared (NIR, 808 nm) irradiation. The NIR irradiation caused an increase of the solution temperature, inducing ROS production and cell wall damage.

In the present study, we have focused on the design and characterization of multifunctional CDs and investigated their antibacterial activity. Till now, various starting materials and synthetic routes to prepare CDs have been developed. These methods can be classified as top-down [12, 25-29] or bottom-up approaches [13, 30, 31]. Among them, the hydrothermal synthesis is mostly used, because it is a simple and efficient way to prepare CDs [6, 25, 32-36]. Recent studies have demonstrated that biocompatible multifunctional CDs may be prepared by using biological precursors [37-43], called green chemistry concept.

In this work, amine-functionalized carbon dots (CDs-NH_2) were synthesized by a simple hydrothermal treatment of citric acid and ethylenediamine. The primary amine groups on the CDs-NH_2 surface were further used for the covalent linking of ampicillin (AMP), a β-lactam antibiotic, to produce CDs-AMP nanostructures. The immobilization of AMP onto the CDs-NH_2 surface was supported by UV-Vis spectrophotometry, Fourier transform infrared spectroscopy (FTIR), atomic force microscopy (AFM), X-ray photoelectron spectroscopy (XPS), thermogravimetric analysis (TGA), zeta potential and dynamic light scattering (DLS) measurements. The antibacterial activity of CDs-NH_2 and CDs-AMP conjugate with and without visible light illumination was evaluated using the *E. coli* K12 – MG 1655 strain by cell growth measurements, standard plate count method and fluorescence-based cell dead/live assay. Our results demonstrated the potential of CDs-AMP as an effective platform for bacteria eradication. The lowest concentration of AMP necessary to inhibit the growth of *E. coli* cells in the case of

CDs-AMP conjugate (14 µg mL^{-1}) was improved compared to free AMP (25 µg mL^{-1}), indicating the advantage of the CDs-AMP conjugate. In addition, we demonstrated that exposure of CDs-AMP to visible light enhances its bactericidal activity. To the best of our knowledge, there are no reports on the use of a platform that combines the intrinsic photodynamic properties of CDs with the antibacterial function of antibiotics loaded on their surface to inhibit the growth of pathogens. The results from this study highlighted the enhanced stability of AMP loaded on the CDs as compared to free AMP in addition to increased antibacterial activity upon visible light irradiation. The existence of a large panel of antibiotics and precursors for CDs synthesis holds great promise for the development of multifunctional nanostructures for combating bacterial infections.

2. Experimental

2.1. Materials

Citric acid, ethylenediamine, 9,10-anthracenediylbis(methylene)dimalonic acid (ABDA), ampicillin (AMP), *N*-(3-dimethylaminopropyl)-*N′*-ethylcarbodiimide hydrochloride (EDC·HCl), *N*-hydroxysuccinimide (NHS), acetic acid, sodium acetate, ninhydrin, potassium cyanide (KCN), pyridine, phenol, quinine sulfate, Hoechst 33342, and paraformaldehyde were purchased from Sigma-Aldrich and used as received.

2.2. Synthesis of amine-functionalized carbon dots (CDs-NH_2)

Amine-functionalized carbon dots were synthesized following a method similar to that reported by Zhu *et al.*[44]. In brief, citric acid (2.1 g) and ethylenediamine (670 µL) were dissolved in Milli-Q water (20 mL). Then the mixture was transferred into a Teflon-lined autoclave (125 mL acid digestion vessel no. 4748, Parr, France) and heated at 250 °C for 5 h. The resulting product was cooled to room temperature and dialyzed against Milli-Q water using a cellulose ester dialysis membrane for 3 days (Biotech CE N°131093, pore size 500-1000 Da) in order to remove unreacted small molecules. Then, dry mass of 200 µL solution was weighted by Sartorius microbalance (TG 209 F3 Tarsus, Netzsch). The yield was about 60 % and the stock solution was stored at 4 °C.

2.3. Conjugation of ampicillin onto amine-functionalized carbon dots (CDs-AMP)

Ampicillin was dissolved in PBS at a concentration of 1 mg mL^{-1}. The carboxyl groups of ampicillin were activated with an equimolar of EDC·HCl and NHS for 30 min. CDs-NH_2 dissolved in PBS at a concentration of 1 mg mL^{-1} and the ampicillin solution were mixed at a volume ratio of 2/1 at room temperature overnight. After that, CDs-AMP conjugate solution was dialyzed (Biotech CE N°131093, pore size 500-1000 Da) against Milli-Q water to remove unreacted ampicillin and kept at 4 °C until use.

2.4. Characterization

Atomic force microscopy (AFM) measurements (NT-MDT Solver Pro-M type apparatus) were carried out in ambient air, in the tapping (non-contact) mode, using commercial standard silicon-nitride tip with a radius of approximately 10 nm (NT-MDT NGS01/Au). The sample was prepared by dropping an aqueous CDs-NH_2 suspension onto a silicon surface and dried at 37 °C.

Size and zeta-potential measurements were performed using a Zetasizer Nano-ZS (Malvern Instruments Inc. Worcestershire, UK). CDs-NH_2 were diluted to 10 µg mL^{-1} and measured in Milli-Q water at pH 7.0.

UV-Vis spectroscopic measurements were carried out using a Perkin Elmer Lambda UV/Vis 950 dual-beam spectrophotometer operating at a resolution of 1 nm. The UV-Vis spectra were recorded in quartz cuvettes of 1 cm path length between 200 and 800 nm.

Emission fluorescence spectra were recorded between 220 and 800 nm using a Cary Eclipse spectrometer (Agilent, France). Solutions were excited from 300 to 400 nm in a 20 nm increment excitation (excitation and emission slit: 5 nm, scan rate: 600 nm/min).

Thermogravimetric analysis (TGA) was carried out on a TG 209 F3 Tarsus Netzsch in the temperature range of 30 to 980 °C using an Al_2O_3 crucible under nitrogen flow (20 mL min^{-1}) with a heating rate of 10 °C/min.

Fourier transform infrared (FTIR) spectra were recorded using a ThermoScientific FTIR instrument (Nicolet 8700) in the range between 650 and 4000 cm^{-1} at a spectral resolution of 6 cm^{-1}. 1 mg of dried CDs-NH_2 was mixed with 200 mg of KBr powder in an agar mortar. The mixture was pressed into a pellet under 7 tons of load for 2-4 min, and the spectrum was recorded immediately. A total of 64 accumulative scans were collected. The signal from a pure KBr pellet was subtracted as a background.

X-ray photoelectron spectroscopy (XPS) measurements were performed with a Theta Probe spectrometer (Thermo Fisher Scientific) spectrometer using a monochromatic Al Kα X-ray source (1486.6 eV) under a vacuum of about 2×10^{-6} Pa at a photoelectron take-off angle of 45 °.

SEM images of pathogens were recorded using a Zeiss Compat Merlin instrument and secondary electron detector at 2 and 5 kV under high vacuum. The biological samples were fixed with 1% glutaraldehyde solution for 30 min in the dark at room temperature and then coated with 5 nm platinum.

2.5. Quantum yield measurements

The fluorescence quantum yield of CDs-NH_2 (in PBS) was determined by the slope method [44] by comparing the integrated photoluminescence intensity and absorbance of each sample with that of a reference. Quinine sulfate (0.1 M H_2SO_4 as a solvent; QY = 0.54) was chosen as the reference. The quantum yield was calculated using the following equation:

$$\phi_x = \phi_{st} (K_x/K_{st}) (\eta_x/\eta_{st})^2$$

where ϕ is the quantum yield, K is the slope determined by the curves and η is the refractive index of the solvent. The subscript "st" refers to the standard with the known quantum yield and "x" for the sample. In order to minimize re-absorption effects, absorption in the 10 mm fluorescence cuvette was kept below 0.10 at the excitation wavelength (360 nm). For these aqueous solutions, $\eta_x/\eta_{st}=1$. A series of concentrations of the reference and sample were measured to obtain the slopes of the curves.

2.6. Quenching of CDs-NH_2 fluorescence in solution

Different concentrations of ampicillin were mixed with CDs-NH_2 and after 12 h, the fluorescence spectra of the samples were recorded at 350 nm excitation wavelength.

2.7. Quantification of primary amine groups by a modified Kaiser test

The primary amine groups were quantified using a modified photometric assay based on the Kaiser test [45]. Briefly, the amine-functionalized CDs-NH_2 powder (0.25 – 1 mg mL^{-1}) was dissolved in 1 mL Milli-Q water. To this suspension was added 1 mL of the buffer solution (1) and then sonicated for 15 min. After that, 1 mL of KCN solution (2) and 1 mL of phenol solution

(3) were added and the suspension was heated at 120 °C for 10 min; 1 mL of ninhydrin solution (4) was added and heated for another 10 min. After the solution was cooled to room temperature, 5 mL of ethanol were added (5).

1. *Buffer solution:* 36 g of sodium acetate were dissolved in 6.9 mL of acetic acid and filled with Milli-Q water until a volume of 100 mL.
2. *KCN solution*: 2 mL of 0.03 M KCN solution were diluted to a volume of 100 mL with pyridine.
3. *Phenol solution*: 80 g of phenol were dissolved in 20 mL of ethanol.
4. *5 % ninhydrin solution*: 5 g of ninhydrin were dissolved in 100 mL of ethanol.
5. *60 % ethanol solution*.

2.8. Singlet oxygen ($^1O_2$) detection

Singlet oxygen generation was measured through the chemical oxidation of an aqueous solution of 9,10-anthracenediylbis(methylene)dimalonic acid (ABDA, 10 µM) in presence of CDs-NH_2 under visible light irradiation. The decrease in the ABDA absorbance at 262 nm was monitored at several time intervals. The light emitted by a visible lamp (Spot Light Source, 420 – 700 nm, L9566-03, Hamamatsu, Japan) was focused onto a quartz cuvette (1 cm path length and 2 mm width) containing 1 mL of the solution. The intensity of the light was measured using a PM600TM laser Fiber Power Meter (Coherent Inc., USA). All the experiments were performed in triplicate.

2.9. Cell culture, cytotoxicity assay and cellular uptake

Cytotoxicity assay

The HeLa cell line, derived from cervical carcinoma from a 31 year old female [ATCC® CCL-2™, ECACC, Sigma Aldrich, Saint-Quentin Fallavier, France] was cultured and maintained in Dulbecco's Modified Eagle's medium (DMEM, Gibco®) supplemented with 10% fetal bovine serum (FBS, Gibco®) and 1% penicillin-streptomycin (Gibco®) in a humidified incubator at 37 °C and 5% CO_2. Cells were seeded at a density of 10^4 cells/well in a 96-well plate and grown for 24 h before assay. The culture medium was replaced with a fresh medium that contains the CDs–NH_2. The final concentration of CDs–NH_2 was 12.5, 25, 50, 100 or 200 µg mL^{-1}. After 24 h, the old medium was aspirated and cells were washed three times with PBS. The cell viability

was evaluated using Uptiblue (Interchim) method. Briefly, 10 µL of the Uptiblue solution were added to each well containing 100 µL of DMEM with 10% FBS and the plate was incubated for 4 h in the humidified incubator. The fluorescence of each well at 590 nm was measured using a microplate reader (PHERAstar FS, BMG LABTECH GmbH, Germany). Each condition was replicated five times and the mean absorbance value of non-exposed cells was taken as 100% cellular viability.

Cell imaging

HeLa cells were seeded in a 24-well plate with sterile coverslips at the bottom at a density of 2×10^5 cells/well and grown for 24 h before assay. The CDs-NH_2 solution was diluted to a final concentration of 200 µg mL^{-1} by DMEM without serum. After incubation for 1 h at 37 °C and 4 °C, the HeLa cell monolayer was washed three times with PBS, fixed on a glass slide with 4% paraformaldehyde at room temperature for 15 min and then stained with 5 µg mL^{-1} DAPI in PBS at room temperature in the dark for 5 min. After gentle washing with PBS (3 times), the coverslips were mounted on glass slides and observed using a Leica AF6000X fluorescence microscope equipped with an Andor iXon 885 Camera and by using an oil immersion objective (100×; 1.4 NA objective). The fluorescence signal was acquired using a dual band excitation and emission filter sets for DAPI ($\lambda_{ex}/\lambda_{em}$: 350/460 nm) and green fluorescent protein (GFP) ($\lambda_{ex}/\lambda_{em}$: 492/534 nm). All the images were further processed using Leica LAS AF Lite software.

2.10. The antibacterial activity of CDs-AMP conjugate

Bacteria growth conditions

A single *E. coli* K12 – MG 1655 colony from LB agar plate was inoculated overnight in LB (Luria-Bertani) medium at 37 °C with moderate shaking. The pre-culture was diluted 50-fold and allowed to continue for another 3 - 4 h until the $OD_{600\ nm}$ had reached 0.6-1.

Bacteria cell viability

The antibacterial activity of AMP and CDs-AMP conjugate with or without visible light illumination was assessed using *E. coli* K12 – MG 1655 strain by cell growth measurements based on the optical density at 600 nm and by plating method to quantify the viable cell number.

Briefly, *E. coli* cells were inoculated in LB medium with different concentrations of carbon dots (CDs-NH_2), ampicillin (AMP), ampicillin mixed with CDs-NH_2, and CDs-AMP conjugate at 37 °C for 6 h and the growth was monitored by measuring the absorbance at 600 nm.

A 10-fold dilution series of the bacterial solutions in phosphate buffer saline were spotted in 10 µL aliquots on LB-agar medium. Visual counting of the number of colonies upon overnight incubation at 37 ºC allowed reading out the initial and final concentrations of the *E. coli* strain in cfu mL^{-1}. All the experiments were performed in triplicate.

Fluorescence-based Cell Dead/Live assay

The total amount of live and dead bacteria cells was determined with Live/Dead *Bac*Light bacterial viability kit (Invitrogen). The samples were incubated in the dark at room temperature for 15 min with 3 µL of two BacLight stains, a 1:1 mixture of SYTO 9 nucleic acid stain and propidium iodide. Then, 5 µL of the stained bacteria suspension was deposited between a glass slide and a cover slip. The slides were observed using a Leica AF6000 LX fluorescent microscope equipped with an Andor iXon 885 Camera using an oil immersion objective (100×; 1.4 NA objective). The fluorescence signal was acquired using a dual band excitation and emission filter sets for green fluorescent protein (GFP) and red fluorescent protein (mCherry). All the images were further processed using Leica LAS AF Lite software.

3. Results and Discussion

Synthesis and characterization of CDs-AMP conjugate

The strategy employed for the synthesis of the carbon dots is illustrated in **Figure S1**. It is based on the hydrothermal approach using citric acid as a carbon source and ethylenediamine as a surface passivation agent. This simple and efficient synthetic route leads directly to amine-functionalized CDs. Moreover, the presence of primary amine groups in the CDs structure expands their application field through conjugation of therapeutic molecules.

We selected ampicillin, a β-lactam antibiotic, as an antibacterial model drug, owing to its broad spectrum range of bactericidal activity. The conjugation of AMP to the CDs-NH_2 surface was achieved through the reaction of the carboxyl group of AMP with the amine groups of the CDs using EDC/NHS as cross-linking agents.

The prepared CDs before and after conjugation with ampicillin (AMP) were characterized using atomic force microscopy (AFM) in tapping mode (**Fig. S2**). Under our experimental conditions, AFM imaging revealed the formation of round shape nanoparticles with an average height of 6 ± 2 nm. After chemical functionalization of the CDs-NH_2 with ampicillin, the average height increased to 41 ± 3 nm, mostly due to CDs' partial aggregation.

According to DLS measurements, the CDs-NH_2 aqueous solution displays an average hydrodynamic diameter of 3.2 ± 0.8 nm (**Fig. S3**). After conjugation with AMP, the average size of CDs-AMP reached 44 ± 10 nm, which is much larger than that of as-prepared CDs-NH_2 due most likely to the formation of aggregated structures, similar to those reported in ref.[15]. The DLS measurements agree well with the AFM results.

The mean zeta potential of the CDs-NH_2 varied from a positive (+16 ± 3 mV) to a negative (-17.5 ± 3 mV) value with the pH varying from 3 to 8. The isoelectric point of the carbon dots was determined to be around 3.7, which is quite similar with previously reported data [46, 47]. In addition, the surface zeta potential changed after the functionalization of the CDs-NH_2 with ampicillin at pH 7.0 from +14 ± 2 mV to -8 ± 2 mV (**Table S1, Fig. S4**).

It should be pointed out that the CDs-NH_2 remain stable in aqueous medium for at least two months at 4 °C without visible precipitation or a decrease in absorbance/fluorescence intensity (**Fig. S5**).

The UV-Vis and fluorescence spectra of CDs-NH_2 and CDs-AMP conjugate are depicted in **Figure 1A.** UV-vis absorption spectrum of CDs-NH_2 exhibits three bands at 237, 342 and 450 nm due to the $\pi \rightarrow \pi^*$ transition of aromatic C=C bond, $n \rightarrow \pi^*$ transition of the C=O bond and to amine-functionalized surface of the CDs [48-51], while the absorption of ampicillin is below 260 nm.

It should be noted that simple mixing of CDs-NH_2 with free AMP did not have any effect on their fluorescence properties (**Fig. S6**), whereas the conjugation of AMP to CDs-NH_2 surface induced a decrease of fluorescence quantum yield from 32% to 19% **(Fig. 1B)**.

The fluorescence spectra exhibit an excitation (λ_{ex}) independent emission (λ_{em}) behavior, which may originate from the CDs uniform size and from the homogeneous distribution of emissive sites (**Fig. 2**) [52]. The maximum fluorescence intensity was recorded at 445 nm under

340 nm excitation with a full width at half maximum (FWHM) of ~76 nm for CDs-NH_2 and ~82 nm for CDs-AMP conjugate.

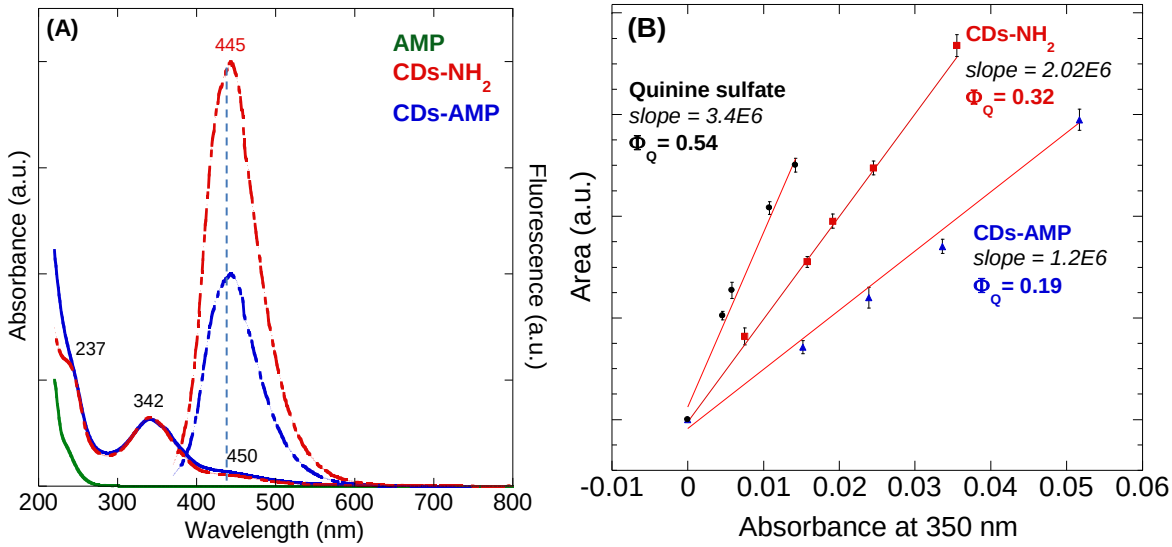

Figure 1. (A) UV-Vis absorption (solid lines) and fluorescence spectra (dash lines, λ_{ex} = 350 nm) of AMP (green), CDs-NH_2 (red) and CDs-AMP conjugate (blue) aqueous solutions. **(B)** Plots of integrated fluorescence spectra against absorbance of quinine sulfate of CDs-NH_2 and CDs-AMP conjugate in PBS. The error bars represent the standard deviation of three independent experiments.

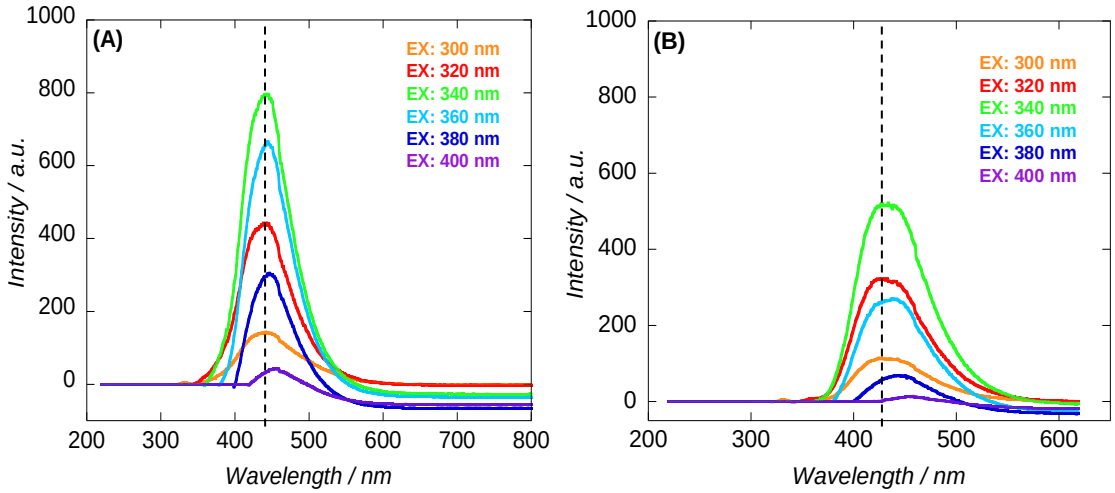

Figure 2. Fluorescence spectra of **(A)** CDs-NH_2 and **(B)** CDs-AMP conjugate for different λ_{ex} wavelengths from 300 to 400 nm with a 20 nm increment.

The thermal properties were probed through thermogravimetric analysis (TGA) measurements (**Fig. S7**). From the TGA results, the amount of AMP conjugated on the surface of the CDs-NH_2 was estimated to be 14%, corresponding to a loading efficiency of 28%. A comparable result was reported by Krishana*et al.*[15]; the amount of ciprofloxacin conjugated onto 1 mg CDs modified glutamic acid was quantified as 96 μg (~10 %). As can be seen in **Fig. S7**, the CDs-AMP conjugate decomposes at a faster rate compared to as-prepared CDs-NH_2 with a maximum weight loss recorded between 150 and 450 °C, indicating the conjugation of AMP to CDs-NH_2 surface.

The FTIR and XPS measurements were carried out to gain further insights into the chemical composition of as-prepared and AMP functionalized CDs-NH_2. In the FTIR spectrum (**Fig. S8**), we can identify the characteristic absorption bands corresponding to stretching vibrations of O-H (3650-3200 cm^{-1}), aromatic C-H (3080-3030 cm^{-1}), aliphatic C-H (3000-2840 cm^{-1}), C=O (1800-1650 cm^{-1} for carboxylic acids and β-lactones), C-C (1297 cm^{-1}), C-O (1126 cm^{-1}) and C-S (700 cm^{-1}). The absorption bands associated with the stretching and deformation vibrations of C-S, NH_2, C=O and C-N (from β-lactam) reflect the conjugation of AMP onto CDs-NH_2. The existence of amine-containing functional groups is confirmed by the stretching vibration and deformation bands of ν_{C-N}, $\nu_{C=N}$ and ν_{N-H}/δ_{N-H} centered at 3250, 1640, 1558, 1395, 1313, 764 and 735 cm^{-1}, respectively.

The presence of primary amine groups is also validated by high-resolution XPS spectrum of the N_{1s} region (**Fig. S9**) and a modified Kaiser test. According to the modified Kaiser test, the –NH_2 surface loading is about 0.7 mmol g^{-1}, meaning that the maximum loading of AMP is 0.245 g per 1 g CDs (**Fig. S10**). From the TGA measurements, the amount of AMP conjugated onto 1 g CDs-NH_2 was quantified as 0.14g, therefore the reaction yield is 57%.

The XPS results are summarized in **Table S2**. Three peaks at 285.1, 399.1 and 532.1 eV revealing the presence of carbon, nitrogen and oxygen, respectively, were observed in all the XPS survey spectra. The additional peak in the XPS survey spectrum of CDs-AMP conjugate, assigned to S_{2p}, clearly indicates the successful conjugation of AMP to CDs surface.

The high resolution spectrum of the S_{2p} region of CDs-AMP shows the presence of –C-S-C- and –C-$S(O)_x$-C-units, centered at 162.3 and 167.4 eV, respectively (**Fig. 3A**). The–C-S-C- unit

displays two peaks at 161.7 and 163.1 eV assigned to $S_{2p3/2}$ and $S_{2p1/2}$ splitting of the S_{2p} spin orbital, respectively. The presence of oxidized sulfur (S-O) suggests that ampicillin was partially oxidized. To rule out the possibility of CDs to oxidize AMP, we have recorded the XPS spectra of AMP powder (**Fig. S11**) and AMP solution (drop casted onto a silicon substrate) (**Fig. 3C**). While the high resolution XPS spectrum of the S_{2p} region of AMP powder displays only non-oxidized sulfur, the S_{2p} high resolution XPS spectrum of AMP that has been previously solubilized in an aqueous medium exhibits both non and oxidized components of sulfur. It is assumed that sulfur oxidation takes place upon the preparation of AMP solution (**Fig. 3C**) (it is generally recommended by the supplier to use AMP solution just after its preparation to limit its degradation).

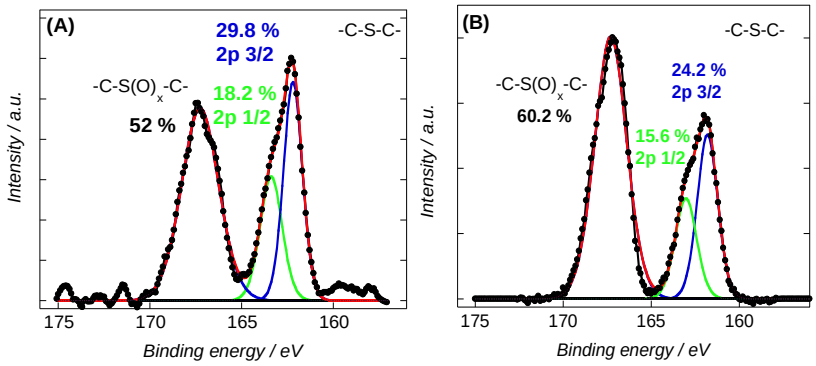

Figure 3. High resolution spectra of S_{2p} of (**A**) CDs-AMP conjugate, and (**B**) a solution of AMP drop casted onto a silicon substrate.

The C_{1s} peak was deconvoluted into three main components assigned to sp^2 C-C at 284.5 eV, oxygen/nitrogen and/or sulfur bonded carbon at 285.5 eV, and C=O/C=N at 288.0 eV for both CDs-NH_2 and CDs-AMP conjugate (**Fig. S12**).

As evidenced from the FTIR and XPS results, the as-synthesized CDs contain a large number of functional groups, including oxygen- and amino-containing groups.

Antibacterial properties

Before investigating the effect of the CDs-NH_2 and CDs-AMP nanostructures on *E. coli* cells, their cytotoxicity and cellular uptake were evaluated on mammalian (HeLa) cells. As can be seen in **Fig. 4,** the amine-functionalized carbon dots can be easily internalized into the cells, crossing

the cell membrane and spreading into the cytoplasm, with reduced toxicity. In agreement, with cytotoxicity study, no significant changes in cell viability were observed upon incubation of the cells with various CDs-NH_2 concentrations ranging from 12.5 to 200 µg mL^{-1} (**Fig. S13**). It was found that more than 90% of cells survive even at a nanoparticle concentration of 200 µg mL^{-1} after 24 h. Similarly, AMP, CDs-AMP and AMP (15%) mixed with CDs did not show any apparent cytotoxicity for concentrations up to 200 µg mL^{-1} (**Fig. S13**). The results clearly indicate that CDs-NH_2 and CDs-AMP are suitable for biomedical applications.

In order to elucidate the uptake mechanism, 200 µg mL^{-1} of CDs-NH_2 were incubated with HeLa cells at 37 °C and 4 °C for 1 h, followed by staining of the nucleus with Hoechst 33342 (blue) and analysis by fluorescence microscopy (**Fig. 4**). Upon incubation of HeLa cells with CD-NH_2 for 1 h at 37 °C, an apparent internalization of the CDs-NH_2 by HeLa cells was evidenced from the green fluorescence homogeneously distributed in the cytoplasm. This contrasts with the lower fluorescence intensity recorded upon incubation for 1 h at 4 °C, because at this temperature, active uptake processes are normally arrested. The green fluorescence observed in the cytoplasm at 4 °C suggested that a small portion of the CDs-NH_2 was internalized by passive penetration. The reduction in the fluorescence signal indicates that cellular uptake of CDs-NH_2 was not determined by a single mechanism; both passive penetration and endocytosis mechanism were responsible for cellular internalization of CDs-NH_2. Wang et *al.*[53] demonstrated that 6 nm mercaptosuccinic acid-coated CdTe quantum dots (MSA-QDs) entered the cells mainly by endocytosis, while part of the 2 nm QDs entered the cells by passive penetration.

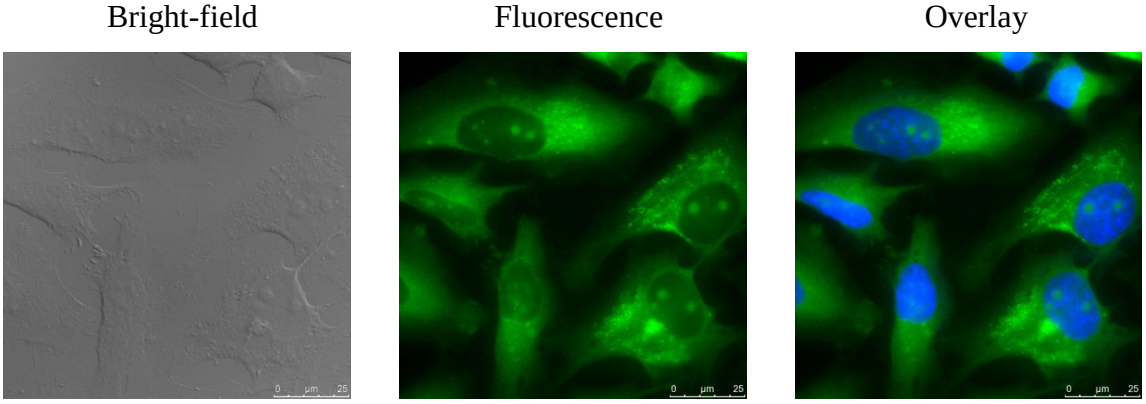

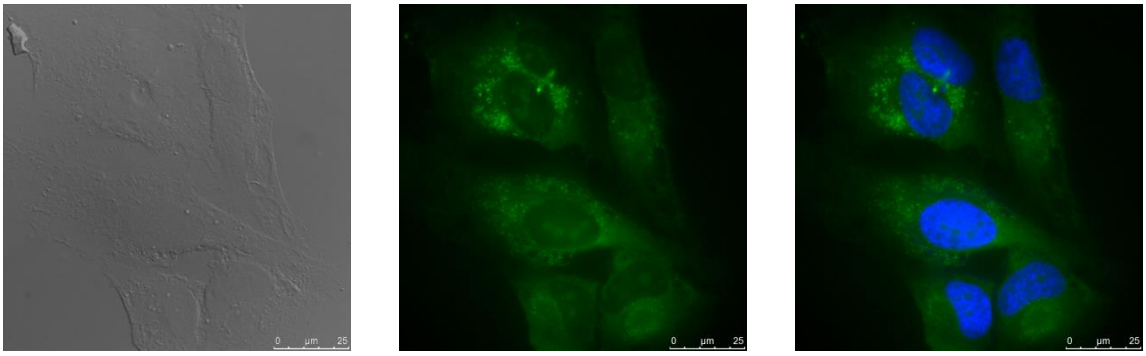

Figure 4. Fluorescence microscopy images of HeLa cells incubated with 200 µg mL^{-1} of CDs-NH_2 for 1 h at 37 °C (**upper**) and 4 °C (**lower**). The green signal in all images corresponds to the amine-functionalized carbon dots; the nuclei of the cells incubated with CDs-NH_2 were stained with Hoechst 33342 (blue).

The antibacterial properties of CDs-NH_2 and CDs-AMP conjugate with or without visible light illumination were evaluated using *E. coli* K12 – MG 1655 strain by cell growth measurements based on the optical density at 600 nm, by plating method to quantify the viable cell number, and fluorescence-based cell dead/live assay; the green fluorescence correspond to live cells while the red fluorescence to dead cells. The fluorescence images in **Fig. 5** revealed that the amine-functionalized carbon dots were not toxic, the bacterial cells remained viable upon exposure to 100 µg mL^{-1} CDs-NH_2 for 6 h. In contrast to CDs-NH_2, the CDs-AMP exerted a pronounced bactericidal activity on *E. coli*. Furthermore, because of the bacterial membrane destruction, it was difficult to image them, the PI cannot penetrate bacterial membrane. This was additionally evidenced by SEM imaging, showing membrane disruption (Inset in **Fig. 5**).

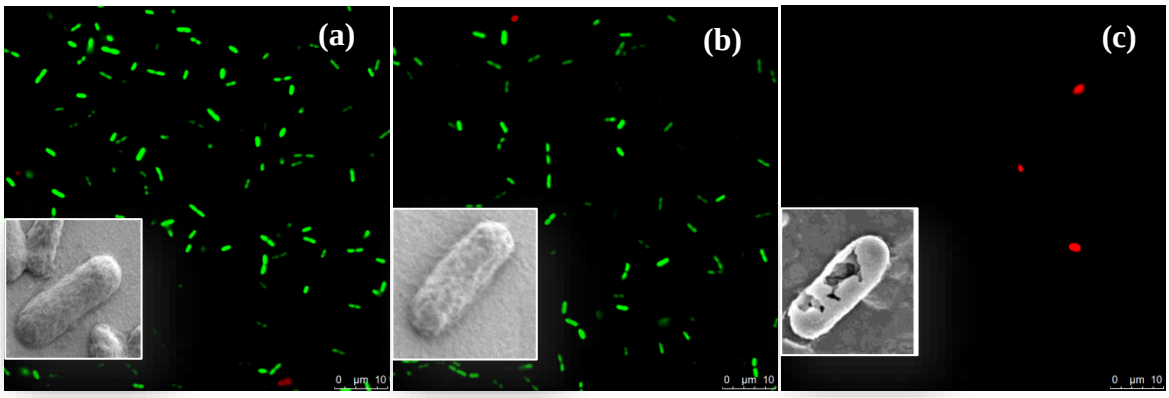

Figure 5. Viability of *E. coli* K12-MG 1655 imaged by the LIVE/DEAD® BacLight™ assay for (a) control - without CDs, (b) with CDs-NH_2 (100 µg mL^{-1}) and (c) with CDs-AMP (100 µg mL^{1}). Inserts: SEM images of bacterial cell.

The covalent attachment of AMP to the CDs surface did not affect its antibacterial activity, but improved its efficacy through MIC reduction by 44% when compared to free AMP (**Fig. 6A**). Indeed, the lowest concentration of AMP necessary to inhibit the visible growth of *E. coli* cells in the case of CDs-AMP conjugate was 14 µg mL^{-1} as compared to 25 µg mL^{-1} using free AMP (**Fig. 6B**). The enhanced antibacterial activity of the CDs-AMP conjugate can be ascribed to its affinity to bind onto the bacterial cell wall which is more easily exposed to a large number of antibiotics molecules, causing its disruption, as can be seen in **Fig. 5**. It is known that the action mode of AMP is associated with cell wall synthesis, inhibiting the activity of the transpeptidase enzyme [54]. Our results are comparable to the reported data in the literature. It is found that the hybrid system comprising nanoparticles and antibiotics exhibited enhanced bactericidal activity and higher stability compared to free antibiotic drugs [16, 55-58].

The result was also confirmed by the antibacterial studies; compared with free AMP, the AMP conjugated onto CDs was still active against *E. coli* cells even after two weeks of storage at 4 °C in aqueous solution (**Fig. S14**). Similar results were reported by Rai *et al.*[59]; Au NPs increased the stability of cefaclor, preserving intact the antibacterial activity for 5 days, while after 9 h the activity of pure cefaclor in solution was only 11%.

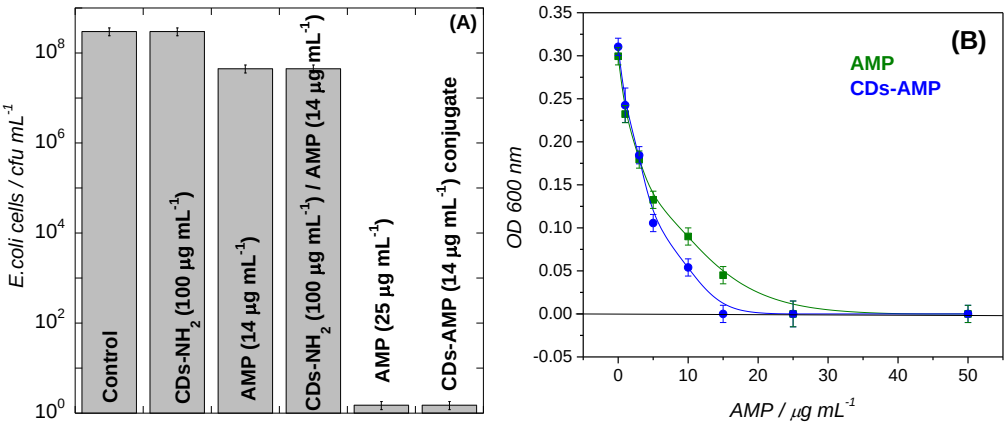

Figure 6. (A) Comparison of the antibacterial activity of CDs-NH_2, free AMP, AMP mixed with CDs-NH_2 with respective to CDs-AMP conjugate against *E. coli* K12 – MG 1655. **(B)** Change of

OD_{600nm} after 6 h in the absence and presence of various concentrations of AMP (0 – 100 µg mL^{-1}). The error bars represent the standard deviation of three independent experiments.

Antibacterial properties under visible light irradiation (PDT)

Furthermore, we have investigated the ability of CDs-NH_2 and CDs-AMP to generate singlet oxygen ($^1O_2$) under visible light illumination for antimicrobial particle–based photodynamic therapy (PPDT). The results indicated that the amount of $^1O_2$ increased with exposure time and visible light lamp intensity (**Fig. S15A**).

The efficiency of CDs-NH_2 and CDs-AMP to kill bacterial cells was investigated by irradiating a suspension of *E. coli* K12 – MG 1655 (1 x 10^6 cfu mL^{-1}) in the presence of CDs-NH_2 and CDs-AMP at different concentrations for 10 or 20 min at 0.3 W.

As seen in **Fig. 7**, the photodynamic bacterial killing effect of CDs-NH_2 depends on the concentration of CDs-NH_2; at a concentration of 400 µg mL^{-1}, the CDs-NH_2 were able to reduce *E. coli* cells viability by 4 log_{10} after 20 min of irradiation. This is in agreement with the amount of singlet oxygen produced using CDs-NH_2. A similar result was reported by Meziani *et al.*[10]

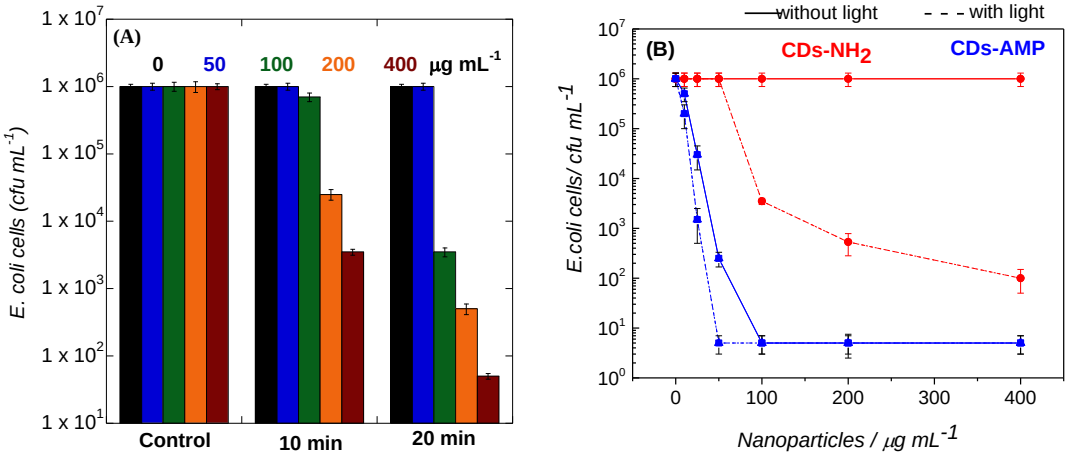

Figure 7. (**A**) Photodynamic efficiency of CDs-NH_2 for the inactivation of *E. coli* K12-MG 1655 upon irradiation at 0.3 W for 10 and 20 min. **(B)** Influence of the CDs-NH_2 and CDs-AMP concentration on the treatment efficiency of *E. coli* without (solid lines) and with (dash lines) visible light illumination (20 min, 0.3 W). The error bars represent the standard deviation of three independent experiments.

Furthermore, the exposure of CDs-AMP to visible light enhanced the bactericidal activity of the conjugate (**Fig. 7B**). The generation of ROS species by the CDs-NH_2, including singlet oxygen ($^1O_2$) may be a possible explanation for the substantial enhancement of the bactericidal activity of CDs-AMP. The CDs-AMP conjugate retained partially the intrinsic theranostic properties of CDs-NH_2, as show in **Fig. S15B**. Therefore, the CDs-AMP conjugate can be used as a multifunctional nanoplatform based on the combined therapeutic killing of antibiotic with visible light triggered photodynamic effects.

4. Conclusion

In summary, carbon dots show considerable potential in biomedical applications, particularly for bacteria eradication. The data presented here demonstrated that amine-functionalized carbon dots (CDs-NH_2) can be successfully used as antimicrobial agent and/or as carrier for the delivery of antimicrobial drugs. Ampicillin-modified CDs were found to be very effective in killing *E. coli* cells, due to the antibacterial function of the ampicillin, combined with the advantage of antimicrobial photodynamic therapy of the CDs. The immobilization of AMP to CDs surface improved its stability and enhanced its bactericidal activity. Furthermore, the photodynamic properties of the CDs enhanced more their bactericidal function upon visible light irradiation. A possible explanation for the effective bacteria killing could be the affinity of CDs to attach on the *E. coli* cells wall, which is more easily exposed to the action of drug molecules and to oxygen reactive species (e.g. singlet oxygen), causing the disruption of cell membrane integrity.

Acknowledgements

Financial support from the Centre National de la Recherche Scientifique (CNRS), the University of Lille, the Hauts-de-France region, the CPER “Photonics for Society”, the Agence Nationale de la Recherche (ANR) and the EU union through FLAG-ERA JTC 2015-Graphtivity, and the Marie Sklodowska-Curie action (H2020-MSCA-RISE-2015, PANG-690836) are acknowledged. We kindly thank Dr. Corentin Spriet, Bio Imaging Center Lille and Dr. David Fournier, UMET, for providing the technical environment to perform the confocal and fluorescence measurements, respectively.

References

[1] V. Turcheniuk, V. Raks, R. Issa, I.R. Cooper, P.J. Cragg, R. Jijie, N. Dumitrascu, L.I. Mikhalovska, A. Barras, V. Zaitsev, R. Boukherroub, S. Szunerits, Diamond Related Mater., 57 (2015) 2-8.

[2] S. Boulahneche, R. Jijie, A. Barras, F. Chekin, S.K. Singh, J. Bouckaert, M.S. Medjram, S. Kurungot, R. Boukherroub, S. Szunerits, J. Mater. Chem. B, 5 (2017) 6557-6565.

[3] R. Jijie, T. Dumych, L. Chengnan, J. Bouckaert, K. Turcheniuk, C.-H. Hage, L. Heliot, B. Cudennec, N. Dumitrascu, R. Boukherroub, J. Mater.Chem. B, 4 (2016) 2598-2605.

[4] H. Maaoui, R. Jijie, G.-H. Pan, D. Drider, D. Caly, J. Bouckaert, N. Dumitrascu, R. Chtourou, S. Szunerits, R. Boukherroub, J. Colloid Interface Sci., 480 (2016) 63-68.

[5] K. Turcheniuk, C.-H. Hage, J. Spadavecchia, A.Y. Serrano, I. Larroulet, A. Pesquera, A. Zurutuza, M.G. Pisfil, L. Héliot, J. Boukaert, J. Mater. Chem. B, 3 (2015) 375-386.

[6] C.-I. Weng, H.-T. Chang, C.-H. Lin, Y.-W. Shen, B. Unnikrishnan, Y.-J. Li, C.-C. Huang, Biosens. Bioelectron., 68 (2015) 1-6.

[7] S. Nandi, M. Ritenberg, R. Jelinek, Analyst, 140 (2015) 4232-4237.

[8] Q. Wang, X. Huang, Y. Long, X. Wang, H. Zhang, R. Zhu, L. Liang, P. Teng, H. Zheng, Carbon, 59 (2013) 192-199.

[9] L. Cao, S.-T. Yang, X. Wang, P.G. Luo, J.-H. Liu, S. Sahu, Y. Liu, Y.-P. Sun, Theranostics, 2 (2012) 295-301.

[10] M.J. Meziani, X. Dong, L. Zhu, L.P. Jones, G.E. LeCroy, F. Yang, S. Wang, P. Wang, Y. Zhao, L. Yang, ACS Appl. Mater. Interfaces, 8 (2016) 10761-10766.

[11] V.N. Mehta, S. Jha, S.K. Kailasa, Mater. Sci. Eng. C, 38 (2014) 20-27.

[12] Y.-P. Sun, B. Zhou, Y. Lin, W. Wang, K.A.S. Fernando, P. Pathak, M.J. Meziani, B.A. Harruff, X. Wang, H. Wang, J. Am. Chem. Soc., 128 (2006) 7756-7757.

[13] D. Zhong, Y. Zhuo, Y. Feng, X. Yang, Biosens. Bioelectron., 74 (2015) 546-553.

[14] Q. Dou, X. Fang, S. Jiang, P.L. Chee, T.-C. Leed, X.J. Loh, RSC Adv., 5 (2015) 46817-46822.

[15] A.S. Krishna, C. Radhakumary, M. Antony, K. Sreenivasan, J. Mater. Chem. B, 2 (2014) 8626-8632.

[16] M. Thakur, S. Pandey, A. Mewada, V. Patil, M. Khade, E. Goshi, M. Sharon, J. Drug Delivery, 2014 (2014) 282193.

[17] C.-W. Lai, Y.-H. Hsiao, Y.-K. Peng, P.-T. Chou, J. Mater. Chem., 22 (2012) 14403-14409.
[18] N. Gogoi, D. Chowdhury, J. Mater. Chem. B, 2 (2014) 4089-4099.
[19] C. Fowley, N. Nomikou, A.P. McHale, B. McCaughan, J.F. Callan, Chem. Commun., 49 (2013) 8934-8936.
[20] Y. Choi, S. Kim, M.H. Choi, S.R. Ryoo, J. Park, D.H. Min, B.S. Kim, Adv. Funct. Mater., 24 (2014) 5781-5789.
[21] W. Bing, H. Sun, Z. Yan, J. Ren, X. Qu, small, 12 (2016) 4713-4718.
[22] J. Liu, S. Lu, Q. Tang, K. Zhang, W. Yu, H. Sun, B. Yang, Nanoscale, 9 (2017) 7135-7142.
[23] J. Yang, X. Zhang, Y.-H. Ma, G. Gao, X. Chen, H.-R. Jia, Y.-H. Li, Z. Chen, F.-G. Wu, ACS Appl. Mater. Interfaces, 8 (2016) 32170−32181.
[24] N. Sattarahmady, M. Rezaie-Yazdi, G. H. Tondro, N. Akbari, J. Photochem. Photobiol. B, 166 (2017) 323-332.
[25] X. Xu, R. Ray, Y. Gu, H.J. Ploehn, L. Gearheart, K. Raker, W.A. Scrivens, J. Am. Chem. Soc., 126 (2004) 12736-12737.
[26] P. Juzenas, A. Kleinauskas, P. George Luo, Y.-P. Sun, Appl. Phys. Lett., 103 (2013) 063701.
[27] W.C. Huang, P.J. Tsai, Y.C. Chen, Small, 5 (2009) 51-56.
[28] J. Lu, J.-x. Yang, J. Wang, A. Lim, S. Wang, K.P. Loh, ACS Nano, 3 (2009) 2367-2375.
[29] L. Zheng, Y. Chi, Y. Dong, J. Lin, B. Wang, J. Am. Chem. Soc., 131 (2009) 4564-4565.
[30] C. Liu, P. Zhang, F. Tian, W. Li, F. Li, W. Liu, J. Mater. Chem., 21 (2011) 13163-13167.
[31] H. Huang, C. Li, S. Zhu, H. Wang, C. Chen, Z. Wang, T. Bai, Z. Shi, S. Feng, Langmuir, 30 (2014) 13542-13548.
[32] B. Bhushan, S.U. Kumar, P. Gopinath, J. Mater. Chem. B, 4 (2016) 4862-4871.
[33] H. Zhu, X. Wang, Y.-J. Li, Z. Wang, F. Yang, X. Yang, Chem. Commun., (2009) 5118-5120.
[34] S. Karthik, B. Saha, S.K. Ghosh, N.D.P. Singh, Chem. Commun., 49 (2013) 10471-10473.
[35] S. Pandey, A. Mewada, M. Thakur, A. Tank, M. Sharon, RSC Adv., 3 (2013) 26290-26296.
[36] S. Pandey, M. Thakur, A. Mewada, D. Anjarlekar, N. Mishra, M. Sharon, J. Mater.Chem. B, 1 (2013) 4972-4982.
[37] H. Huang, J.-J. Lv, D.-L. Zhou, N. Bao, Y. Xu, A.-J. Wang, J.-J. Feng, RSC Adv., 3 (2013) 21691-21696.

[38] C. Zhu, J. Zhai, S. Dong, Chem. Commun., 48 (2012) 9367-9369.
[39] S. Sahu, B. Behera, T.K. Maiti, S. Mohapatra, Chem. Commun., 48 (2012) 8835-8837.
[40] L. Wang, H.S. Zhou, Anal. Chem., 86 (2014) 8902-8905.
[41] W. Lu, X. Qin, S. Liu, G. Chang, Y. Zhang, Y. Luo, A.M. Asiri, A.O. Al-Youbi, X. Sun, Anal. Chem., 84 (2012) 5351-5357.
[42] S. Liu, J. Tian, L. Wang, Y. Zhang, X. Qin, Y. Luo, A. Asiri, A.O. Al-Youbi, X. Sun, Adv. Mater., 24 (2012) 2037-2041.
[43] Y. Yang, J. Cui, M. Zheng, C. Hu, S. Tan, Y. Xiao, Q. Yang, Y. Liu, Chem. Commun., 48 (2012) 380-382.
[44] S. Zhu, Q. Meng, L. Wang, J.-R. Zhang, Y. Song, H. Jin, K.-Q. Zhang, H. Sun, H. Wang, B. Yang, Angew. Chem. Int. Ed., 52 (2013) 3953-3957.
[45] G. Jarre, S. Heyer, E. Memmel, T. Meinhardt, A. Krueger, Beilstein J. Org. Chem., 10 (2014) 2729-2737.
[46] Z.L. Wu, P. Zhang, M.X. Gao, C.F. Liu, W. Wang, F. Leng, C.Z. Huang, J. Mater. Chem. B, 1 (2013) 2868-2873.
[47] X. Jia, J. Li, E. Wang, Nanoscale, 4 (2012) 5572-5575.
[48] J. Niu, H. Gao, J. Lumin., 149 (2014) 159-162.
[49] H. Wang, P. Gao, Y. Wang, J. Guo, K.-Q. Zhang, D. Du, X. Dai, G. Zou, APL Mater., 3 (2015) 086102.
[50] X. Zhang, Y. Zhang, Y. Wang, S. Kalytchuk, S.V. Kershaw, Y. Wang, P. Wang, T. Zhang, Y. Zhao, H. Zhang, ACS Nano, 7 (2013) 11234-11241.
[51] L. Shi, J.H. Yang, H.B. Zeng, Y.M. Chen, S.C. Yang, C. Wu, H. Zeng, O. Yoshihito, Q. Zhang, Nanoscale, 8 (2016) 14374-14378.
[52] Z. Yang, M. Xu, Y. Liu, F. He, F. Gao, Y. Su, H. Wei, Y. Zhang, Nanoscale, 6 (2014) 1890-1895.
[53] T. Wang, X. Jiang, ACS Appl. Mater. Interfaces, 5 (2013) 1190-1196.
[54] B. Saha, J. Bhattacharya, A. Mukherjee, A. Ghosh, C. Santra, A.K. Dasgupta, P. Karmakar, Nanoscale Research Letters, 2 (2007) 614.
[55] B. Saha, J. Bhattacharya, A. Mukherjee, A. Ghosh, C.R. Santra, A.K. Dasgupta, P. Karmakar, Nanoscale Res. Lett., 2 (2007) 614.

[56] W. Wu, S. Wieckowski, G. Pastorin, M. Benincasa, C. Klumpp, J.P. Briand, R. Gennaro, M. Prato, A. Bianco, Angew. Chem. Int. Ed., 44 (2005) 6358-6362.

[57] A.N. Brown, K. Smith, T.A. Samuels, J. Lu, S.O. Obare, M.E. Scott, Appl. Environm. Microbiol., 78 (2012) 2768-2774.

[58] R. Jijie, A. Barras, F. Teodorescu, R. Boukherroub, S. Szunerits, Mol. Syst. Des. Eng., 2 (2017) 349-369.

[59] A. Rai, A. Prabhune, C.C. Perry, J. Mater. Chem., 20 (2010) 6789-6798.